Front. Mech. Eng. China (2006) 2: 131–145
DOI 10.1007/s 11465-006-0018-y

RESEARCH ARTICLE

Shi-kui CHEN, Michael Yu WANG

Conceptual design of compliant mechanisms using level set method

Abstract We propose a level set method-based framework for the conceptual design of compliant mechanisms. In this method, the compliant mechanism design problem is recast as an infinite dimensional optimization problem, where the design variable is the geometric shape of the compliant mechanism and the goal is to find a suitable shape in the admissible design space so that the objective functional can reach a minimum. The geometric shape of the compliant mechanism is represented as the zero level set of a one-higher dimensional level set function, and the dynamic variations of the shape are governed by the Hamilton-Jacobi partial differential equation. The application of level set methods endows the optimization process with the particular quality that topological changes of the boundary, such as merging or splitting, can be handled in a natural fashion. By making a connection between the velocity field in the Hamilton-Jacobi partial differential equation with the shape gradient of the objective functional, we go further to transform the optimization problem into that of finding a steady-state solution of the partial differential equation. Besides the above-mentioned methodological issues, some numerical examples together with prototypes are presented to validate the performance of the method.

keywords compliant mechanisms, conceptual design, level set methods, shape gradient, Hamilton- Jacobi PDE

I Introduction

Mechanisms play a role of utmost importance in machinery. They are capable of transmitting motion, force and energy to meet design requirements [1]. According to the intrinsic way of transferring force and motion, the category of mechanisms can be subdivided into rigid-body mechanisms and compliant mechanisms. The former, in general, consists of numerous parts connected by rigid joints, where force and motion are transmitted by the relative motion between these joints. Different from rigid-body mechanisms, compliant mechanisms, usually in a monolithic form, transmit energy and motion from specified input ports to output ports by the elastic deformation of its comprising material [2]. Because of this property, compliant mechanisms by nature possess some inherent advantages over their rigid-body counterparts. They can be manufactured with small dimensions, light weights and ease in assembly as well [3]. In the same way, compliant mechanisms provide people with effective means of eliminating back lash, wear and friction which are often associated with rigid-body mechanisms. These merits have proven especially valuable in microelectromechanical systems(MEMS) [4], [7], high precision instruments [5] and medical tools for minimally invasive surgery [6].

It is rather difficult to quote the exact date of invention of compliant mechanisms. But the record of their application can be traced back to the early stage of human history [1]. And for a long time, the design procedure was rather a handicraft than a technology. The traditional design of compliant mechanisms is made on an ad hoc basis, which to a large extent depends on the designers' intuition, experience and inspiration. The limitations of such a trial-and-error approach are obvious: it is not always guaranteed to work, especially when the design is very complicated or when topology and multi-material problems are taken into account. The practical design and application of compliant mechanisms are in need of a systematic and effective approach to create conceptual designs.

Directed toward this goal, various scientific endeavors have been made by different research groups during the past decades. In general, the major design approaches fall into two categories. The first approach, represented by Howell and Midha [1], [12], has its roots in the concept of flexible linkages [8]. The basic configuration of an analogous rigid-body mechanism is first obtained based on kinematic synthesis. Then by replacing the rigid-body linkages with

Shi-kui CHEN(✉) Michael Yu WANG
Computational Modeling and Design Laboratory,
Department of Automation and Computer-Aided Engineering,
The Chinese University of Hong Kong,
Shatin, N.T., Hong Kong, China
Email: skchen@ acae.cuhk.edu.hk

compliant joints, the basic rigid-body configuration can be transformed into that of a compliant mechanism. A genuine defect of this approach lies in the fact that even with rigorous analysis the compliant design may not be able to fully reproduce the motion of its rigid body counterpart.

The second category of approaches is mainly based on the design techniques originally developed for structural optimization. These methods include ground structure method, homogenization method (and its variant SIMP method), and level set methods [2], [3], [20], [24], [26], [27]. The underlying idea of these methods is to recast the design problem as an optimal material distribution problem so that the configuration of the design can fulfill the requirements measured quantitatively by an objective function. The differences among these approaches lie in their representations and modeling schemes.

In the ground structure method, the design is represented by a full or a modular ground structure. In the optimization process, an elastic analysis of the compliant mechanism is implemented iteratively using truss elements or frame elements. Based on the results of the elastic analysis, bars with cross sections reduced to a lower threshold are removed gradually.

In contrast to the ground structure method representing material in a discrete form, homogenization-based methods are distributed material optimization methods [9], which have been a main approach to structural optimization. In this method, the structure to be optimized is fixed in a reference domain and is discretized with the elements for elastic analysis. The design variables are the artificial densities of the elements and their material properties are modeled in terms of a set of material interpolation functions such that the intermediate properties are penalized usually using a 'power-law' applied on the relative material density. A limitation of the homogenization methods is that the results are always in a check-board pattern, and some post processes are usually needed before the results are put into practical use.

The level set approach, possessing a boundary representation geometric model, was initially proposed by Osher and Sethian on a physical base to solve the boundary-capturing problem in computational fluid dynamics [16]. And in the past twenty years, level set methods have been successfully extended to versatile application areas [29], [30]. Sethian and Wiegmann first combined level set methods with immersed interface methods to do structural boundary design [17], where the former was used to represent the boundary of the design and the latter was used to do elastic analysis. Different from Sethian and Wiegmann, Osher and Santosa introduced the shape gradient of the objective functional into the level set model, establishing a link between the shape gradient and the velocity field [18]. Recently, the work was further consummated by Wang [27] and Allaire [20]. What's more, Wang proposed a '**color level set**' model, and thus made possible topology optimization with multi materials in the level set framework [2], [25].

The rest of the paper is organized as follows: Section 2 describes the setting of the problem. Section 3 introduces several basic issues in the level set methods. Section 4 gives the shape gradient of the objective functional (geometric advantage). Section 5 presents the flow chart of the algorithm and some numerical examples. Some prototypes will be presented in the last section to assess the performance of this method.

2 Problem formulation

As mentioned in the previous section, a compliant mechanism should be capable of transmitting motion and energy from the input port to the output port. And this functional requirement is specified in quantity by an objective function. In terms of topology optimization of a compliant mechanism, the most frequently used objective functions include: a weighted sum of mutual strain energy (MSE) and strain energy (SE), the ratio of MSE to SE [21], geometric advantage, mechanical advantage and work efficiency [10], [22]. The study of the effects of the above-mentioned objective functions on the final designs is beyond the scope of this paper. Here, we just follow Sigmund's way [10] to select geometric advantage as our choice for the objective function. The geometric advantage (GA) of compliant mechanisms is defined as follows (as shown in Fig. 1):

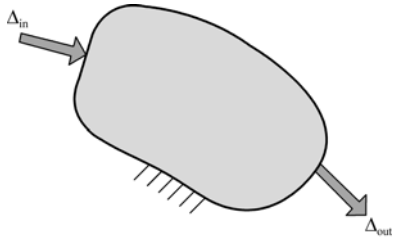

Fig. 1 A schematic of a compliant mechanism with input displacement and output displacement

$$GA(u,\Omega) = -\frac{\Delta_{\text{out}}(u,\Omega)}{\Delta_{\text{in}}(u,\Omega)} \tag{1}$$

where Δ_{out} and Δ_{in} denote the displacements at the output port and the input port, respectively; $\Omega \subseteq R^d (d = 2 \text{ or } 3)$ represents an open and bounded set occupied by a linear isotropic elastic material, and it is also the design variable in the level-set-based shape optimization framework; u is the external force-induced displacement field in Ω.

With the objective function, the original design problem is transformed into a conventional optimization problem. Our task is to find a proper shape from the admissible design space, so that the objective function can reach its minimum. However, only with the objective function, the topology optimization problem is usually ill posed, that is, the optimum solution is not always guaranteed to exist. To

regularize the ill-posed optimization problem, some extra constraints should be put into consideration. The usually used constraints are volume constraint and perimeter constraint [9]. Besides these, stress is another important issue needing great concern in the optimization design procedure. This constraint is applied indirectly by limiting the range of the input displacement [10]. Combining the constraints with objective function (1), we can specify the general problem of compliant mechanism optimization as

$$\begin{aligned} &\underset{\Omega}{\text{Minimize}}\ J(u,\Omega)=GA(u,\Omega)+\mu\left|\partial\Omega\right| \\ &\text{subject to}\ \int_{\Omega}\mathrm{d}\Omega\leqslant[V]_{\max} \\ &\qquad\Delta_{\text{in}}(\Omega)\leqslant[\Delta_{\text{in}}]_{\max} \\ &\int_{D}E_{ijkl}\varepsilon_{ij}(u)\varepsilon_{kl}(v)H(-\phi)\mathrm{d}\Omega=\int_{\partial\Omega}f\cdot v\mathrm{d}s \\ &\qquad u\big|_{Td}=0,\forall v\in U \end{aligned} \tag{2}$$

where μ is a positive parameter, $\partial\Omega$ denotes the boundary of the elastic material, and $\left|\partial\Omega\right|$ is the perimeter of the boundary. The last constraint equation is the weak form of the linear elastic equation governing the linear elastic structure of the compliant mechanism.

3 Level set model

Since its being introduced by Osher and Sethian as a scheme for following fronts propagating with curvature-dependent speed [16], level set model has thrived to be a powerful tool with many applications in different fields [29], [30]. Its charm lies in giving a natural way to describe closed boundaries with dynamics variations, and enabling easy '*capture*' of the boundary on a Euler grid by solving a Hamilton-Jacobian partial differential equation. In order not to be lost in technical detail, in this section, we will give a brief introduction only to those key issues involved in topology optimization of compliant mechanisms. For a complete introduction on level set methods, please refer to [29], [30].

3.1 Implicit representation of the boundary

Just as its name implies, level set method implicitly represents the boundary as the zero level set of a one-higher dimensional surface $\phi(x)$, which is called level set function. In the level set model, the domain is defined as three parts according to the value of the level set function:

$$\begin{cases}\phi(x(t))>0:\forall x(t)\in D\setminus\Omega\\ \phi(x(t))=0:\forall x(t)\in\partial\Omega\\ \phi(x(t))<0:\forall x(t)\in\Omega\setminus\partial\Omega\end{cases} \tag{3}$$

where D denotes the design domain; and $t\in R^{+}$ is time. The domain and the level set embedding of the model are shown in Fig. 2. The greatest advantage of implicit representation lies in the fact that it is able to deal with topological changes, such as splitting and merging of the boundary, in a natural manner. And in addition, with implicit representation, boolean operations on the boundary are easy to implement. With the level set model, we can rewrite the problem formulation as:

$$\begin{aligned} &\underset{\phi}{\text{Minimize}}\ J(u,\phi)=GA(u,\phi)+\mu\int_{D}\delta(\phi)\left|\nabla\phi\right|\mathrm{d}\Omega \\ &\text{subject to}\ \int_{D}H(-\phi)\mathrm{d}\Omega\leqslant[V]_{\max} \\ &\qquad\Delta_{\text{in}}(\Omega)\leqslant[\Delta_{\text{in}}]_{\max} \\ &\int_{D}E_{ijkl}\varepsilon_{ij}(u)\varepsilon_{kl}(v)H(-\phi)\mathrm{d}\Omega=\int_{\partial\Omega}f\cdot v\mathrm{d}s \\ &\qquad u\big|_{Td}=0,\forall v\in U \end{aligned} \tag{4}$$

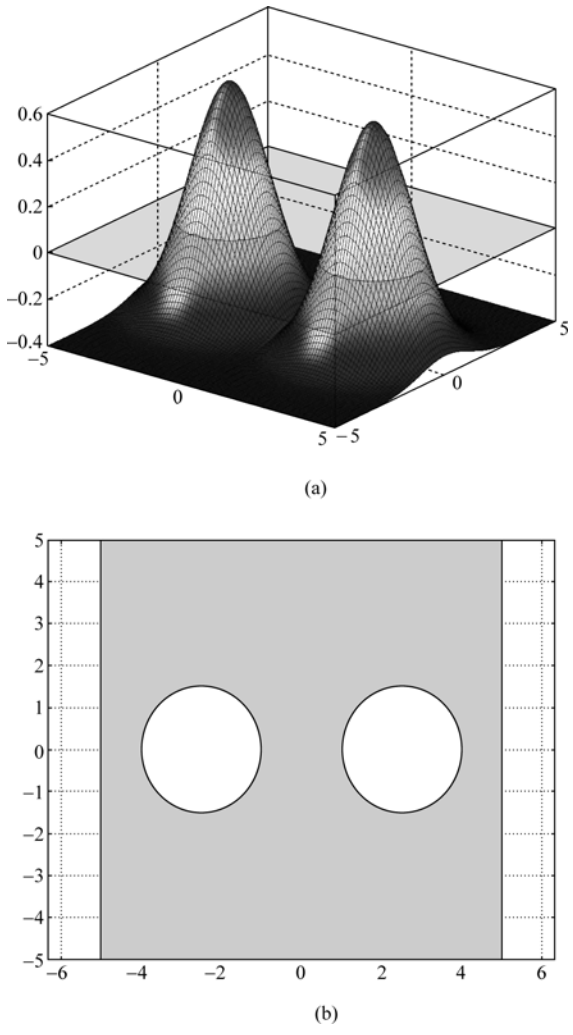

Fig. 2 A 2D boundary embedded as the zero level set of a 3D level set function. **a** The implicit level set function. **b** Its corresponding boundary

where $H(\phi)$ is the Heaviside function defined as follows:

$$H(\phi)=\begin{cases}1, if\ \phi\geqslant 0\\ 0, if\ \phi<0\end{cases} \tag{5}$$

and $\delta(\phi)$ is the one dimensional delta function:

$$\delta(\phi) = \frac{dH}{d\phi} \tag{6}$$

3.2 Level set equations and its numerical computation

1. Governing equation for boundary variations As presented in subsection A, the boundary is embedded as the zero level set of the level set function. During the optimization process the level set surface may move up and down on a fixed Euler grid, and thus causing the embedded boundary to undergo drastic shape or topological changes. From beginning to end, the value of the level set function on the boundary is constantly kept to be zero, viz.

$$\phi(x) \equiv 0, \forall x \in \partial\Omega \tag{7}$$

If we differentiate the above equation with respect to time t, we can get the follow equation with the chain rule:

$$\frac{\partial\phi}{\partial t} + \nabla\phi \cdot V(x) = 0 \tag{8}$$

where $V(x) = \frac{\mathrm{d}x}{\mathrm{d}t}$ is the velocity vector field. Considering $n = \frac{\nabla\phi}{|\nabla\phi|}$ and $V \cdot \nabla\phi = (V \cdot n)|\nabla\phi|$, we can write Eq. (8) as

$$\frac{\partial\phi}{\partial t} + V_n |\nabla\phi| = 0 \tag{9}$$

These two Hamilton-Jacobi type partial differential equations are the well-known level set equations [16], [29], [30]. Based on the level set theory, the topology optimization problem is transformed into a problem of finding the steady-state solution of the Hamilton-Jacobi equation. As we can see from Eqs. (8) and (9), after the initial level set function $\phi(x)$ is identified, to get a feasible steady-state solution, the crux is to find a meaningful velocity field. We will mention this in a later section.

2. Discrete computation scheme: The discrete solution to the Hamilton- Jacobi equation is acquired by using an **upwind difference scheme**' [29], [30]. The upwind scheme adaptively calculates forward or backward difference at a point according to the direction of the velocity field at that point. In our understanding, the underlying idea of the upwind scheme is that information is always spreading from the known area to the unknown area, and what the upwind scheme does is to use the information in the known area to speculate about that in the unknown area.

The following is the first-order upwind scheme for 2D cases:

$$\begin{aligned}\phi_{ij}^{n+1} = \phi_{ij}^{n} - \Delta t(&\max((V_n)_{ij}, 0)\nabla^{+} \\ &+ (\min((V_n)_{ij}, 0)\nabla^{-}\end{aligned} \tag{10}$$

where

$$\begin{aligned}\nabla^{+} = \{&\max(D_{ij}^{-x}, 0)^2 + \min(D_{ij}^{+x}, 0)^2 \\ &+ \max(D_{ij}^{-y}, 0)^2 + \min(D_{ij}^{+y}, 0)^2\}^{1/2} \\ \nabla^{-} = \{&\max(D_{ij}^{+x}, 0)^2 + \min(D_{ij}^{-x}, 0)^2 \\ &+ \max(D_{ij}^{+y}, 0)^2 + \min(D_{ij}^{-y}, 0)^2\}^{1/2}\end{aligned}$$

Δt is the time step, and it should satisfy the Courant-Friedrichs-Lewy (CFL) conditions [29]:

$$\Delta t \leqslant \frac{\min(\Delta x, \Delta y)}{\max|(V_n)_{ij}|} \tag{11}$$

Δx and Δy are grid spaces in horizontal and vertical directions, $D_{ij}^{\pm x}$, $D_{ij}^{\pm y}$ are forward (+) and backward (–) finite difference operators.

3.3 Calculation of geometric quantities

In the optimization process, it is often necessary to approximate some quantities, e.g., the normal vector, curvature, perimeter, area, etc. In the level set model, all these geometric quantities can be expressed as functions in terms of the implicit level set function $\phi(\mathrm{x})$. The most-often-used geometric quantities include [29], [30]:

1. Normal vector $\vec{N}$ (pointing in the direction of increasing ϕ),

$$\vec{N} = \frac{\nabla\phi}{|\nabla\phi|} \tag{12}$$

2. The mean curvature *k* of the interface, which is defined as the divergence of the normal vector $\vec{N}$:

$$k = \nabla \cdot \vec{N} = \nabla \cdot \frac{\nabla\phi}{|\nabla\phi|} \tag{13}$$

3. The perimeter of the boundary $|\partial\Omega|$:

$$|\partial\Omega| = \int_D \delta(\phi)|\nabla\phi| d\Omega \tag{14}$$

4. The area of the elastic material $|\Omega|$:

$$|\Omega| = \int_D H(-\phi) d\Omega \tag{15}$$

3.4 Level set surface re-initialization

Theoretically speaking, the implicit level set function can be of any type only if it is a smooth function satisfying Eq. (3). But in practice, to get highly accurate numerical results [16], it is usually regularized as a signed **distance function**, which is a subset of implicit functions and is defined as follows:

$$\phi(x) = \begin{cases} d(x), \forall x \in D \setminus \Omega \\ 0, \forall x \in \partial\Omega \\ -d(x), \forall x \in \Omega \setminus \partial\Omega \end{cases} \tag{16}$$

where $d(x)$ is the distance function defined as:

$$d(x) = \min(|x - x_I|), for\ \forall x_I \in \partial\Omega \quad (17)$$

An important feature of the signed distance function is that $|\nabla\phi(x)| = 1$, $\forall x \in D$. In the optimization process, the level set surface may become too steep or too flat, deviating away from the signed distance function. This may cause numerical instability. So it is necessary to regularize the level set surface to be a signed distance function from time to time. This process is called **re-initialization**. In this paper, we use the PDE-based method proposed by Peng, Merriman and Osher [19], which needs to solve another PDE shown in Eq. (18) for its steady state:

$$\frac{\partial\phi}{\partial t} = \text{sign}(\phi)(1 - |\nabla\phi|) \quad (18)$$

where

$$\text{sign}(\phi) = \begin{cases} 1, if\ \phi > 0 \\ 0, if\ \phi = 0 \\ -1, if\ \phi < 0 \end{cases} \quad (19)$$

In a similar way, we use the upwind finite difference scheme to get the steady-state solution of equation (18) and makes $|\nabla\phi| = 1$ indirectly.

4 Shape gradient and velocity field

To find a minimization solution to the optimization problem, we need to find the variation of the objective function with respect to a variation of the design variable. This process is usually called *sensitivity analysis*. And since in our case the design variable is the shape represented by the level set model, it is also called **shape sensitivity analysis** and the result is called **shape gradient**.

The shape gradient is acquired with a two-step procedure: First, using the linear superposition principle of displacement field and the reciprocity principle [11], we express Eq. (1) in terms of displacement variables u_{1i}, u_{1o}, u_{2i} and u_{2o}, whose definition will be given later. In the second step, based on shape sensitivity theory [31], we derive the shape derivative of the above displacement variables, and further give the shape gradient of the objective function with the chain rule.

The physical property of the compliant mechanism is assumed to be linear elastic. When a unit force f_{in} with the same direction of the input force F_{in} is applied at the input port of the mechanism, it generates a displacement field in the solid. u_1 denotes the displacement field caused by the unit force f_{in}. Let u_{1i} denote the displacement at the input port in the same direction as f_{in}, and u_{1o} denote the displacement at the output port in the same direction as the output force, as shown in Fig. 3(a). The linear elastic equilibrium can be written in the following weak variation form:

$$\begin{aligned} &\int_D E_{ijkl}\varepsilon_{ij}(u_1)\varepsilon_{klv}vH(-\phi(x,t))\mathrm{d}\Omega = f_{\text{in}} \cdot v(20) \\ &u|\Gamma_d = 0, \forall v \in U \end{aligned} \quad (20)$$

where U denotes the admissible displacement field.

In a similar way, when a unit force f_{out} is applied at the output port, we have another linear elastic equilibrium equation similar to Eq. (20):

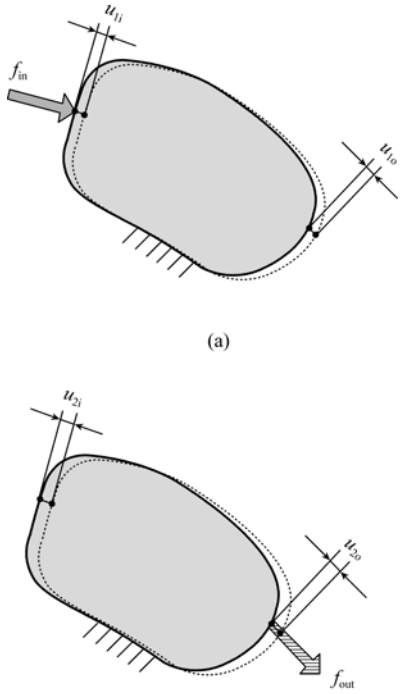

Fig. 3 A schematic of **a** u_{1i} and u_{1o}. **b** u_{2i} and u_{2o}

$$\int_D E_{ijkl}\varepsilon_{ij}(u_2)\varepsilon_{klv}vH(-\phi(x,t))\mathrm{d}\Omega = f_{out} \cdot v \quad (21)$$

where u_2 is the displacement field caused by f_{out}.

Replace v with u_1 and u_2, respectively, in Eq. (20), we can obtain

$$u_{1i} = \int_D E_{ijkl}\varepsilon_{ij}(u_1)\varepsilon_{klv}(u_1)H(-\phi(x,t))\mathrm{d}\Omega \quad (22)$$

$$u_{1o} = \int_D E_{ijkl}\varepsilon_{ij}(u_1)\varepsilon_{klv}(u_2)H(-\phi(x,t))\mathrm{d}\Omega \quad (23)$$

where u_{2i} is the displacement at the input port caused by f_{out}. Note that f_{in} and f_{out} are unit forces.

Similarly, by replacing v with u_1 and u_2, respectively, in Eq. (21) we obtain

$$u_{2o} = \int_D E_{ijkl}\varepsilon_{ij}(u_2)\varepsilon_{kl}(u_2)H(-\phi(x,t))\mathrm{d}\Omega \quad (24)$$

$$u_{2i} = \int_D E_{ijkl}\varepsilon_{ij}(u_2)\varepsilon_{kl}(u_1)H(-\phi(x,t))\mathrm{d}\Omega \quad (25)$$

According to the reciprocity principle, the work done by f_{in} in Eq. (23) is equal to the work done by f_{out} in equation (25), i.e.

$$u_{1o} = u_{2i} = \int_D E_{ijkl}\varepsilon_{ij}(u_1)\varepsilon_{kl}(u_2)H(-\phi(x,t))\mathrm{d}\Omega \quad (26)$$

Since the system is a linear elastic system, the final displacement field can be expressed as the linear superposition of the two displacement fields caused by F_{in} and F_{out} respectively. That is,

$$\begin{aligned} \Delta_{\text{in}} &= F_{\text{in}}u_{1i} + F_{\text{out}}u_{2i} \\ \Delta_{\text{out}} &= F_{\text{in}}u_{1o} + F_{\text{out}}u_{2o} \end{aligned} \quad (27)$$

Further more, it is assumed that there exists a linear relationship between F_{out} and the output displacement [21] as

$$F_{\text{out}} = \Delta_{\text{out}} + f_0 \tag{28}$$

where k and f_{o} are constants. With Eq. (27) and (28), we have the following expressions for Δ_{in} and Δ_{in}

$$\begin{aligned} \Delta_{\text{in}} &= \frac{-F_{\text{in}}u_{1\text{i}} - f_{\text{o}}u_{2\text{i}} - F_{\text{in}}ku_{1\text{o}}u_{2\text{i}} + F_{\text{in}}ku_{1\text{i}}u_{2\text{o}}}{-1+ku_{2\text{o}}} \\ \Delta_{\text{out}} &= \frac{-F_{\text{in}}u_{1\text{o}} - f_{\text{o}}u_{2\text{o}}}{-1+ku_{2\text{o}}} \end{aligned} \tag{29}$$

Then, the geometric advantage can be expressed as

$$GA = -\frac{\Delta_{\text{out}}}{\Delta_{\text{in}}} = \frac{F_{\text{in}}u_{1\text{o}} + f_{\text{o}}u_{2\text{o}}}{-F_{\text{in}}u_{1\text{i}} - f_0u_{2\text{i}} - F_{\text{in}}ku_{1\text{o}}u_{2\text{i}} + F_{\text{in}}ku_{1\text{i}}u_{2\text{o}}} \tag{30}$$

Now the shape gradient of the objective function can be written as

$$\begin{aligned} D_\Omega J = D_\Omega(GA) + \mu D_\Omega(|\partial\Omega|) = \frac{\partial GA}{\partial u_{1\text{i}}}D_\Omega u_{1\text{i}} + \\ \frac{\partial GA}{\partial u_{1\text{o}}}D_\Omega u_{1\text{o}} + \frac{\partial GA}{\partial u_{2\text{i}}}D_\Omega u_{2\text{i}} + \frac{\partial GA}{\partial u_{2\text{o}}}D_\Omega u_{2\text{o}} + \mu D_\Omega(|\partial\Omega|) \end{aligned} \tag{31}$$

For a general functional of the integration of an integrand $g(x)$ on the domain Ω

$$u(\Omega) = \int_\Omega g(x)\mathrm{d}x \tag{32}$$

its shape derivative is known to have the following form [28], [31]

$$D_\Omega u = \oint_{\partial\Omega} g(x)V_n \mathrm{d}s \tag{33}$$

where V_n is the normal velocity of x on the boundary. With Eq. (33), we can get the shape gradient of $u_{1\text{i}}$, $u_{1\text{o}}$, $u_{2\text{i}}$, $u_{2\text{o}}$ and the shape gradient of volume constraint.

The perimeter $|\partial\Omega|$ is an integration along the boundary. Instead of directly using the results given by Sokolowski [31], we use the knowledge from differential geometry to give a brief derivation. The boundary can be regarded as a closed curve $\vec{C}(p) = \{x(p), y(p)\}$, where $p \in [0,1]$. Formally, we say that the curve maps the interval I = [0, 1] to the Euclidean space R^2 and write $C : I \to R^2$

$$\begin{aligned} D_\Omega|\partial\Omega| = \frac{\mathrm{d}}{\mathrm{d}t}|\partial\Omega| = \int_0^1 \frac{\mathrm{d}}{\mathrm{d}t}\left(\left|\vec{C}_p\right|\right)\mathrm{d}p = \int_0^1 \frac{\vec{C}_p}{\left|\vec{C}_p\right|}\left(\vec{C}_{pt}\right)\mathrm{d}p \\ = \frac{\vec{C}_p \cdot \vec{C}_t}{\left|\vec{C}_p\right|}\Big|_{p=0}^{1} - \int_0^1 \vec{C}_t \mathrm{d}\frac{\vec{C}_p}{\left|\vec{C}_p\right|} = -\int_0^1 \vec{C}_t \mathrm{d}\frac{\vec{C}_p}{\left|\vec{C}_p\right|} \end{aligned} \tag{34}$$

Note that $\left.\frac{\vec{C}_p \cdot \vec{C}_t}{\left|\vec{C}_p\right|}\right|_{p=0} = \left.\frac{\vec{C}_p \cdot \vec{C}_t}{\left|\vec{C}_p\right|}\right|_{p=1}$ As we know $\vec{V} = \vec{C}_t = \{xt(p), y_t(p)\}$ and $\vec{T} = \frac{\vec{C}_p}{\left|\vec{C}_p\right|} = \frac{\{x_p, y_p\}}{\sqrt{x_p^2 + y_p^2}}$, where $\vec{T}$ is the unit tangent. So Eq. (34) becomes $\int_0^1 \vec{V}d\vec{T} = \oint_{\partial\Omega} \vec{V}\cdot\vec{T}_s \mathrm{d}s$ As $\vec{T}_s = -\kappa\vec{N}$, then $\oint_{\partial\Omega} \vec{V}\cdot\vec{T}_s \mathrm{d}s = -\oint \kappa\vec{V}\cdot\vec{N}\mathrm{d}s = -\oint \kappa\vec{V}_n \mathrm{d}s$. So the shape gradient of the boundary length

$$D_\Omega(|\partial\Omega|) = \oint_{\partial\Omega} \kappa\vec{V}_n \mathrm{d}s \tag{35}$$

Now substitute the shape gradient of $u_{1\text{i}}$, $u_{1\text{o}}$, $u_{2\text{i}}$, $u_{2\text{o}}$ and the shape gradient of the perimeter $|\partial\Omega|$ into Eq. (31), we can get the shape gradient of the objective function (4) as

$$D_\Omega J = \oint_\Omega GV_n \mathrm{d}\Omega \tag{36}$$

where

$$\begin{aligned} G = \frac{\partial GA}{\partial u_{1\text{i}}}E_{ijkl}\varepsilon_{ij}(u_1)\varepsilon_{kl}(u_1) + \left(\frac{\partial GA}{\partial u_{1\text{o}}} + \frac{\partial GA}{\partial u_{2\text{i}}}\right)E_{ijkl}\varepsilon_{ij}(u_1)\varepsilon_{kl}(u_2) \\ + \frac{\partial GA}{\partial u_{2\text{o}}}E_{ijkl}\varepsilon_{ij}(u_2)\varepsilon_{kl}(u_2) + \mu\kappa \end{aligned} \tag{37}$$

and is known as the shape gradient density [31].

After we get the shape gradient of the objective function, it is natural for us to use the steepest descent optimization process by letting $V_n = -G$ in the Hamilton-Jacobi Eq. (9).

5 Numerical algorithms

We imply topology optimization of compliant mechanism with the following steps:

Step 1: Define the initial level set function and set the initial condition. The initial level set function gives the initial value of the Hamilton-Jacobi PDE, which is also the starting point of the optimization process. Note that the initial level set function has a nontrivial effect on the final optimization result.

Step 2: Elastic analysis. In this step, we solve the linear elastic Eqs. (20) and (21) using finite element analysis and get concerned displacement fields.

Step 3: Sensitivity analysis and definition of the velocity field. Based on the results from elastic analysis, we can calculate the shape gradient density G in Eq. (37), and get the velocity V_n in a further step.

Step 4: Evolve the level set surface. After acquiring the velocity field V_n, we can update the level set surface with the Hamilton-Jacobi Eq. (9).

Step 5: Re-initialization of the level set surface. In order to avoid the level set surface deviating from a signed-distance function, we do surface re-initialization every a few steps using the partial differential Eq. (18).

The above steps (Step 2 - Step 5) are repeated until the convergence criterion is satisfied. The above-mentioned procedure can be expressed by the following flowchart shown in the appendix.

6 Numerical examples

In this section, we show several numerical examples, which include the design for a displacement inverter, a push-gripper, and a push clamp, to assess the performance of our level-set-based design method. These examples are well studied in literatures [1] and [9] with other methods, and thus can be used as benchmarks for our performance evaluation.

6.1 Displacement Inverter

The function of a displacement inverter is sketched in Fig. 4.

The input displacement Δ_{in} is induced by the external force $F_{in} = 50$ applied at the input port, and the output

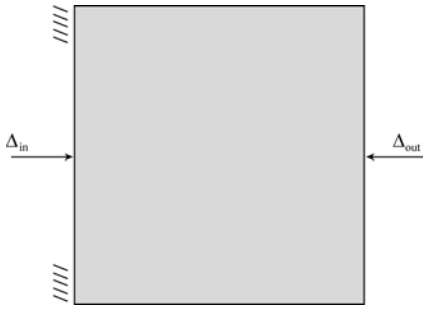

Fig. 4 A schematic of a displacement inverter

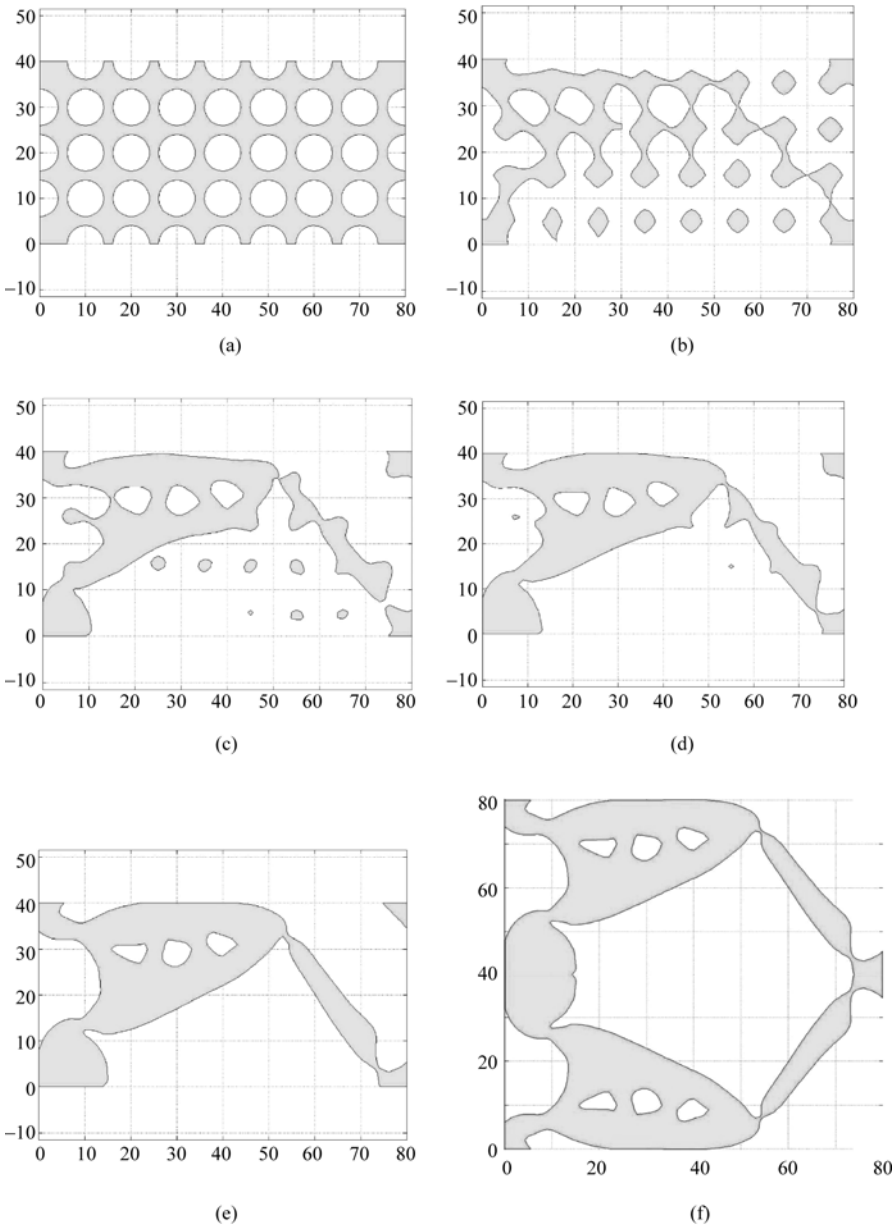

Fig. 5 Iterations for the displacement inverter

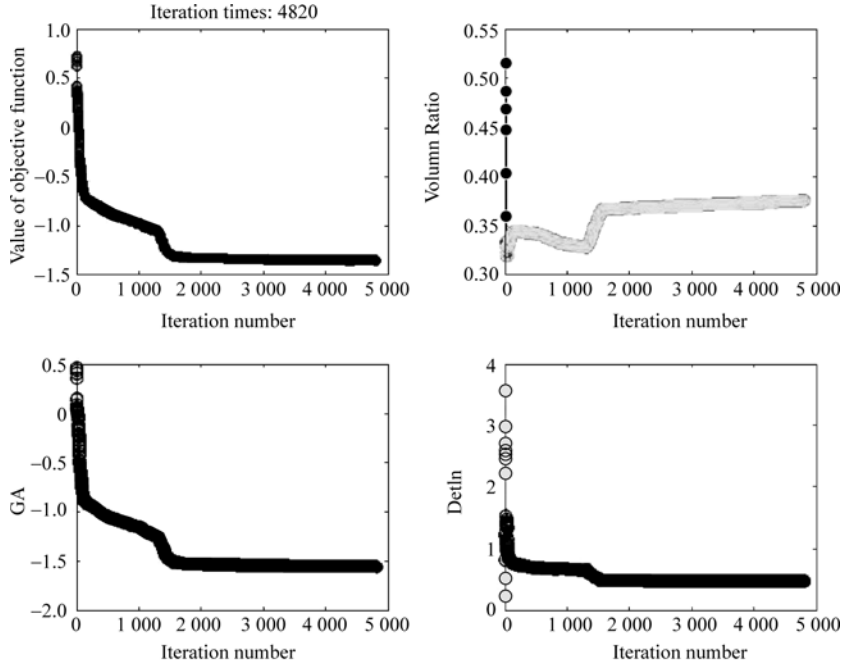

Fig. 6 Changes in objective function J, volume ratio $\frac{V}{V_0}$, geometric advantage GA and input displacement Δ_{in} for the displacement inverter

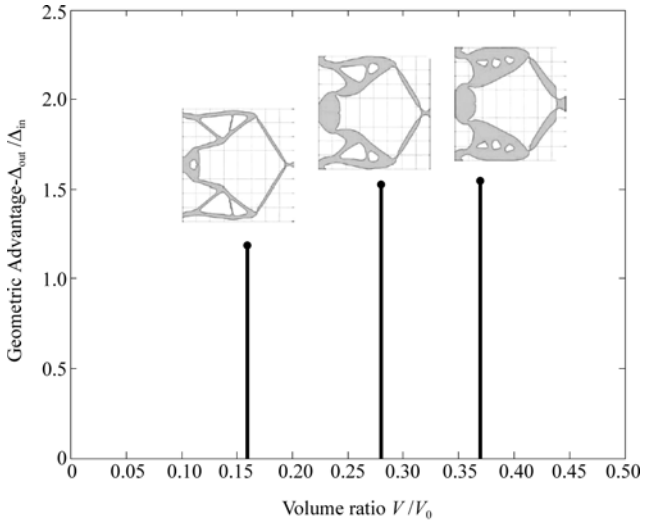

Fig. 7 Designs with different volume constraints

displacement Δ_{out} is produced in a direction opposite to that of Δ_{in}. The design domain is defined within an 80-by-80 square. Due to the symmetry, only the upper half of the mechanism is taken into account and is discretized using 80-by-40 finite elements for elastic Fig. 4. A schematic of a displacement inverter analysis. The elastic material is assumed with a dummy Young's modulus of E = 1 and the Poisson ratio of 0.3. The void area is assumed with a dummy Young's modulus of 0.001 and the same Poisson ratio of 0.3. The Lagrangian multiplier μ for the perimeter is 2×10^{-6}, and the Lagrangian multiplier for the volume constraint is 0.5.

The optimization process is shown in Fig. 5. The initial boundary is represented by Fig. 5(a), the intermediate solutions are shown in Fig. 5(b) – 5(d). The final design is shown in Fig. 5(e) and 5(f). The changes in the objective function J, the material volume ratio $\frac{V}{V_0}$, the geometric advantage GA and the input displacement Δ_{in} are shown in Fig. 6, respectively. We also present designs with different volume constraints in Fig. 7.

6.2 Push-Gripper

We consider a design for a push-gripper in this example. Its function is sketched in Fig. 8, where the mechanism is supported at part of its left side. The input displacement is applied at the middle of the left side, and two vis-à-vis vertical output displacements are expected near the middle of the right side. The design domain is defined in an 80-by-80 square, and the upper half is discretized with 80-by-40 finite element for elastic analysis.

Figure 9(a) – 9(d) show the iteration process and Fig. 9(e)–9(f) show the final result. Figure 10 shows the changes in the objective function, the volume ratio, the geometric advantage and the input displacement.

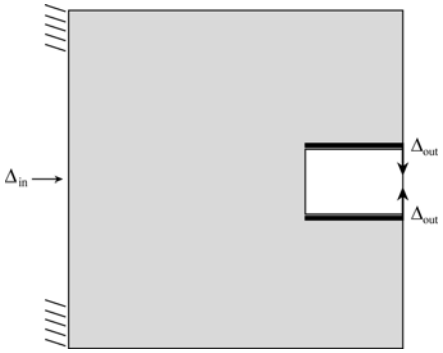

Fig. 8 A schematic of a push-gripper

6.3 Push-Clamp

The design problem for a push-clamp is sketched in Fig. 11, where the mechanism is supported at the left side and is subject to a vertical squeezing load F_{in} = 50 μN at the upper and lower right corners. A clamping force F_{out} is expected at the output port.

A minor difference between this example and the previous two is that here we choose mechanical advantage $MA = \frac{F_{out}}{F_{in}}$ as our objective function instead of geometric

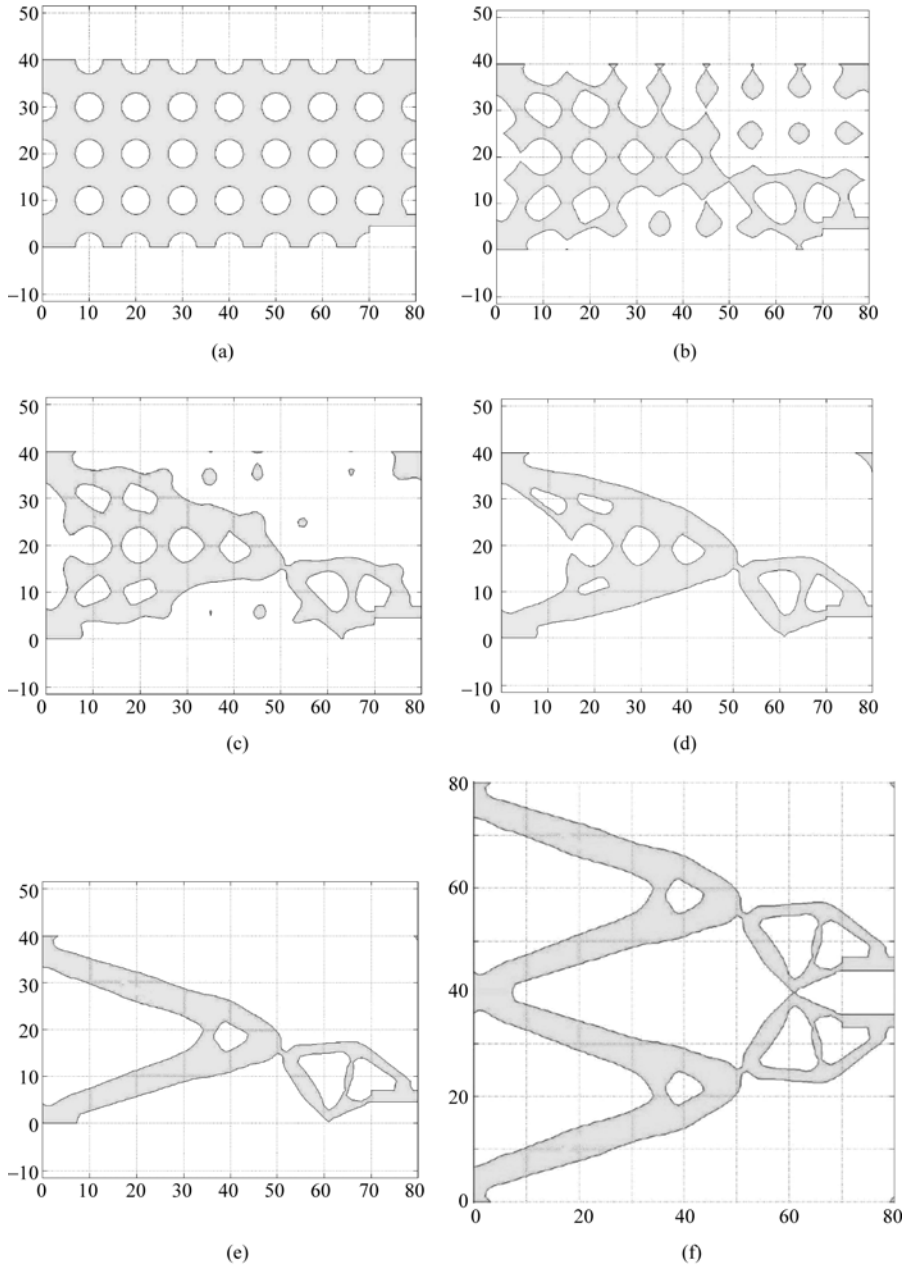

Fig. 9 Iterations for the push-gripper

advantage, but the analysis process is almost the same. The design domain is defined in a 120-by-80 square, and the upper half is discretized with 122-by-42 finite element for elastic analysis. The elastic material is assumed with a dummy Young's modulus of E = 3 GPa and the Poisson ratio of 0.4. The volume constraint is given as $\frac{V}{V_0} = 0.3$, and constraint on the input displacement is $\Delta_{\text{in}} = 0.15\mu m$. Different from example A and B, where the constraints are implemented using a fixed Lagrangian multiplier [20], in this example the constraints are implemented using the gradient projection technique [2].

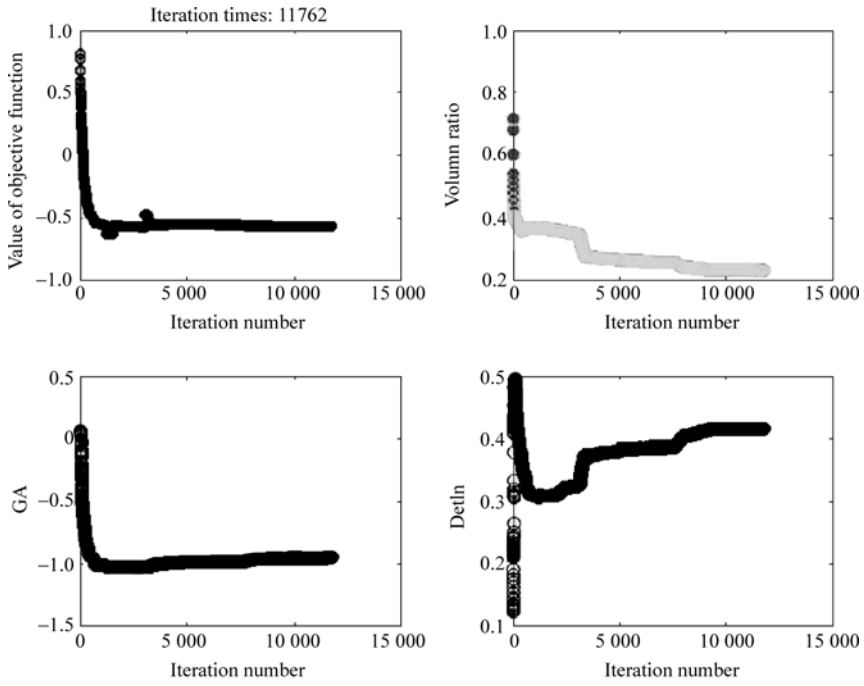

Fig. 10 Changes in objective function J, volume ratio $\frac{V}{V_0}$, geometric advantage GA and input displacement Δ_{in} for the push-gripper

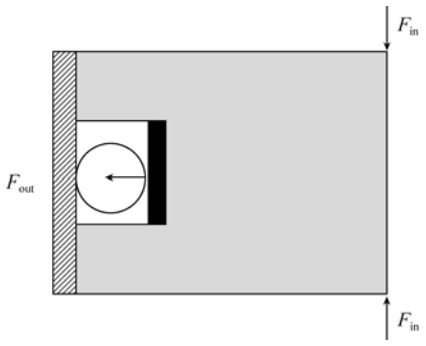

Fig. 11 A schematic of a push-clamp

Figure 12(a) – 12(d) show the iteration process and Fig. 12(e) – 12(f) show the final result. Figure. 13(a) shows the changes in the mechanical advantage, and Fig. 13(b) shows the changes in volume ratio and input displacement.

7 Finite element simulation, demonstration prototypes and experimental tests

In this section, we select the push-clamp as an example for further analysis and experiment. Based on the conceptual design, we construct a CAD model and use it in **Algor FEMPRO** to simulate the displacement and stress field under working conditions. After that, a prototype made of **aluminum 6061-T6** is fabricated using wire EDM. Experimental tests are carried out subsequently to assess its performance.

7.1 Finite element simulation

We convert Fig. 12(f) into a CAD model as shown in Fig.14. The dimension of the CAD model is modified to be 120 mm× 80 mm×3 mm in order to conform to that of the prototype. Then

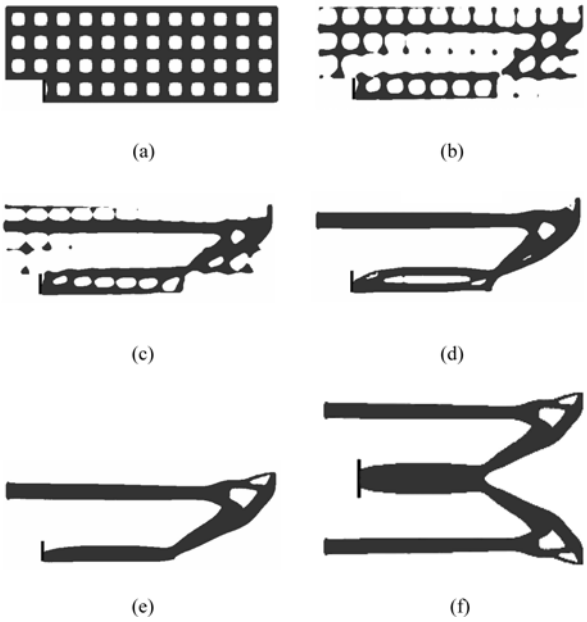

Fig. 12 Iterations for the Push-Clamper

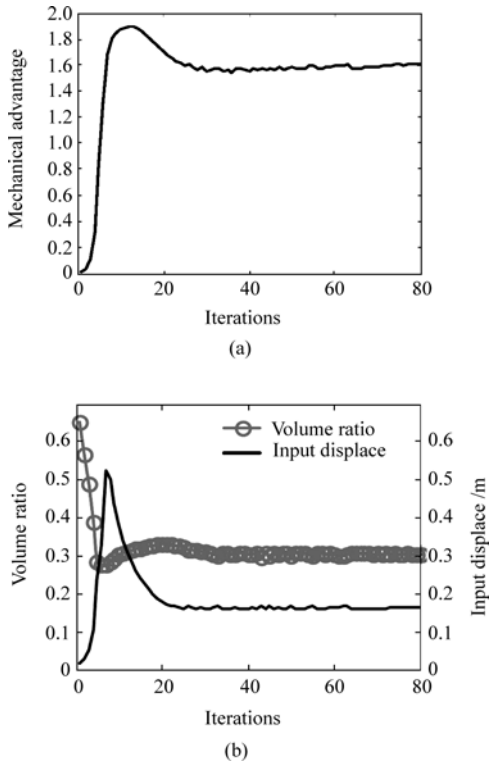

Fig. 13 Changes in **a** geometric advantage *MA*. **b** volume ratio $\frac{V}{V_0}$, and input displacement Δ_{in} for the push-clamp

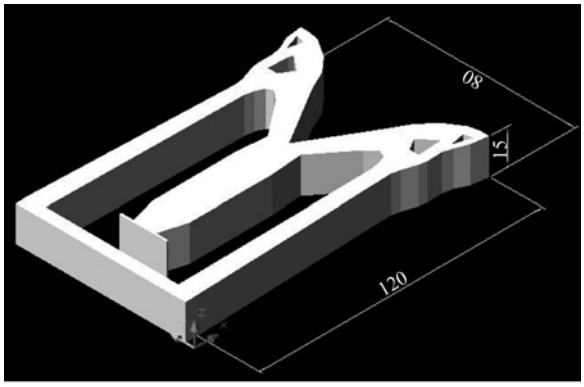

Fig. 14 The CAD model of the push-clamp

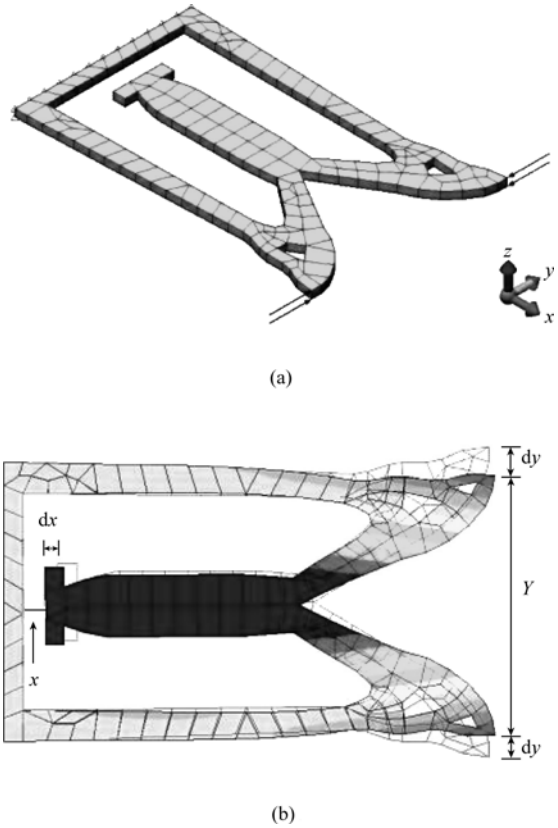

Fig. 15 Settings for finite element simulation. **a** Boundary condition and force condition simulation. **b** A sketch for the parameters

this CAD model is input into Algor for finite element analysis. The material properties are specified as those of aluminum.

The boundary conditions and force conditions are set as Fig.15(a) shows. The concerned test parameters dx, dy, x and y are sketched in Fig.15(b), where dx is the input displacement, dy is the output displacement, x is the distance from the output port to the left side, and y is the distance between the two force-applied tips. The input force F_{in} varies arithmetically from 200 N to 2 000 N with a step of 200 N. The values of the experimental parameters are presented in Table 1.

Table 1 Simulation result for the push-clamp made of aluminum

F_{in}/N	dx/mm	dy/mm	σ_{max}/(N·mm^{-2})
200	0.380	0.789	450.343
400	0.766	1.578	902.686
600	1.149	2.367	1 351.03
800	1.533	3.157	1 801.37
1 000	1.921	3.945	2 251.71
1 200	2.299	4.735	2 702.06
1 400	2.683	5.520	3 152.4
1 600	3.066	6.313	3 602.74
1 800	3.449	7.102	4 053.09
2 000	3.832	7.892	4 503.43

7.2 Prototype and experimental test

The prototype of the push-clamp is fabricated with EDM with the dimension of 120 mm×80 mm×3 mm, as shown in Fig. 16.

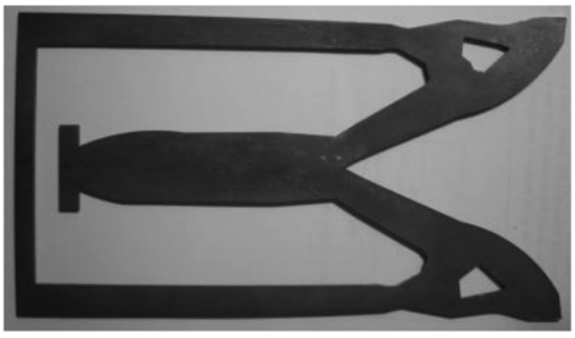

(a)

(b)

Fig. 16 Photos of the prototypes. **a** Planform of the push-clamp. **b** Two push-clamp prototypes with thickness of 1 mm (the lower one) and 3 mm

The experimental test is shown in Fig. 17. The push-clamp is placed horizontally. A fastening clip is used to produce a pair of vis-à-vis forces at the input ports. To avoid failure, an additional red clip is added and fixed with the de-facto axis area where the maximum stress usually appears. With different input displacement dy, the push-clamper will produce a corresponding output displacement dx. The experimental data are presented in Table 2. We plot the input and output displace- ment from computational simulation and experimental test in Fig.18. The geometric advantage evaluated from finite element simulation is 0.486, and that from experimental test is about 0.505. We can see in this case the stimulation results accord well with experiment results. But unfortunately, we have to admit that in some cases the stimulation results deviate from the experiment results. This phenomenon may be caused by various reasons, including the errors in mathematic model, finite element analysis, fabrication process, experiment method, or the high sensitivity of the performance with respect to the shape of the design, which need further studies in future researches.

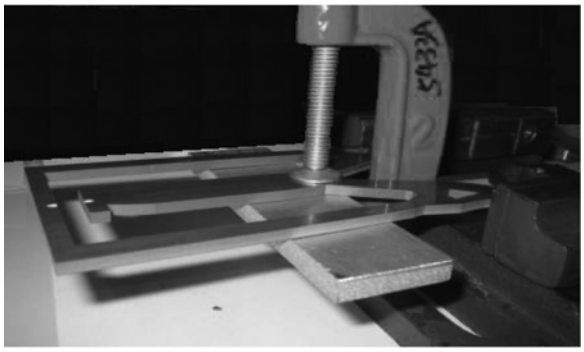

Fig. 17 Experiment setting for the push-clamp

Table 2 Experiment result for the push-clamp made of aluminum

X/mm	Y/mm	dx/mm	dy/mm
9.12	79	0.14	0.5
8.86	78	0.4	1.0
8.58	77	0.68	1.5
8.36	76	0.9	2.0
8.02	75	1.24	2.5
7.76	74	1.5	3.0
7.54	73	1.72	3.5
7.20	72	2.06	4.0
6.98	71	2.28	4.5
6.74	70	2.52	5.0
6.46	69	2.8	5.5
6.22	68	3.04	6.0
5.98	67	3.28	6.5

8 Conclusions

We propose a level-set-method based framework for the conceptual design of compliant mechanisms. In this method, the compliant mechanism design problem is recast as an infinite dimensional optimization problem, where the design variable is the geometric shape of the compliant

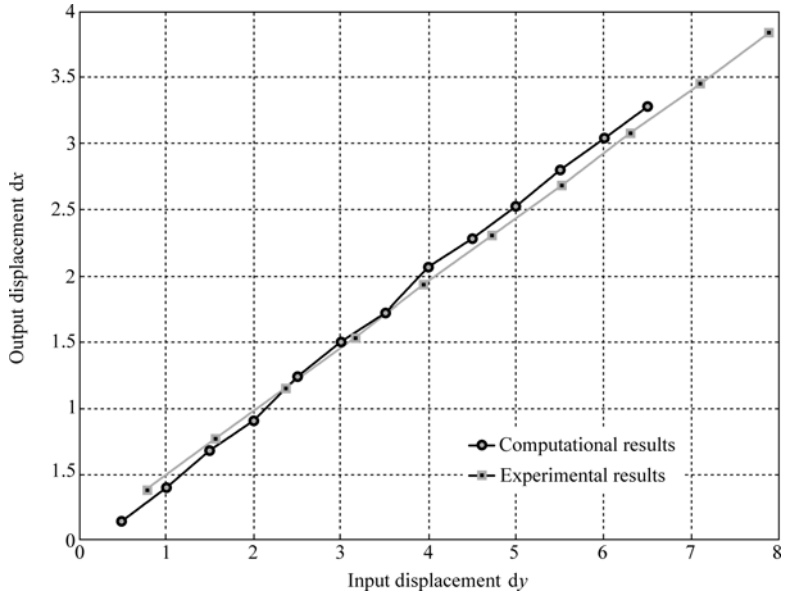

Fig. 18 Comparison of the computational and experimental results

mechanism and the goal is to find a suitable shape in the admissible design space so that the objective functional can reach a minimum. We have shown that the proposed method has a promising advantage in handling topology changes. It provides a robust way for the conceptual design of compliant mechanisms.

Acknowledgements This research work is supported in part by the Research Grants Council of Hong Kong SAR (No. CUHK4164/03E) and the National Natural Science Foundation of China (NSFC) (Project Nos. 50128503, 50305019 and 50390063). We thank Mr. P.K. Lam for performing the FEM analysis, prototype fabrication and experimental testing work.

Appendix

The flowchart of the optimization algorithm(Fig. 19)

References

1. L. L. Howell, Compliant Mechanisms, John Wiley & Sons, New York, 2001
2. M. Y. Wang, S. K. Chen, X. Wang, and Y. Mei, Design of multi-material compliant mechanisms using level set methods, Journal of Mechanical Design, Trans. of ASME, 2005, (127)5, 941–956
3. S. K. Chen, M. Y. Wang, and S. Y. Wang, Optimal synthesis of compliant mechanisms using a connectivity preserving level set method, Proc. of ASME 31st Design Automation Conference, Long Beach, CA, Sep. 2005
4. D. Xu and G.K. Ananthasuresh, Freeform Skeletal Shape Optimization of Compliant Mechanisms, ASME Journal of Mechanical Design, 2003, 125: 253–261.
5. L. Zuo, N. Landsiedel, M. Prakash, M. Kartik, Design of Six-Axis Nano-Manipulator based on Compliant Mechanism, Report, MIT, Dec 2003
6. M. Frecker, R. Dziedzic, and R. Haluck, Design of Multifunctional Compliant Mechanisms for Minimally Invasive Surgery, Minimally Invasive Therapy and Allied Technologies, accepted, 2002
7. S.Kota, J.Joo, Z.Li, Design of Compliant Mechanisms: Applications to MEMS, Analog Integrated Circuits and Signal Processing-An International Journal, 2001, 29:715
8. R. H. Burns and F. Crossley, Structural Permutations of Flexible Link Mechanisms, ASME Paper 1966, 66-Mech-5
9. M. P. Bendsoe and O. Sigmund, Topology Optimization: Theory, Methods and Applications, Springer, 2003
10. O. Sigmund, On the Design of Compliant Mechanisms using Topology Optimization, Mechanics of Structures and Machines, 1997, 25 (4): 493–524
11. N. Lobontiu, Compliant mechanisms: Design of Flexure Joints, CRC Press, 2002, 20
12. L.L. Howell and A. Midha, A method for the design of compliant mechanisms with small-length flexural pivots, ASME Journal of Mechanical Design, 1994, 116: 280–289
13. A. Kawamoto, M. P. Bendsoe and O. Sigmund, Articulated mechanism design with a degree of freedom constraint, International Journal for Numerical Methods in Engineering, 1998, 42: 535–559
14. G. Allaire, F. Jouve, Optimal design of micro-mechanisms by the homogenization method, European Journal of Finite Element, 2002, 11: 405–416
15. M. P. Bendsoe, and N. Kikuchi, Generating optimal topologies in structural design using a homogenization method, Computer Methods in Applied Mechanics and Engineering, 1998, 71: 197–224
16. S. Osher, J.A. Sethian, Fronts propagating with curvature-dependent speed: algorithms based on Hamilton-Jacobi formulations, Journal of Computational Physics 1988, 79: 12–49
17. J.A. Sethian and A. Wingman, Structural Boundary Design via Level Set and Immersed Interface Methods, Journal of Computational Physics, Nov. 1999
18. S. J. Osher, F. Santosa, Level set methods for optimization problems involving geometry and constraints. I. Frequencies of a two-density inhomogeneous drum, Journal of Computational Physics, 2001, 171(1):272–288

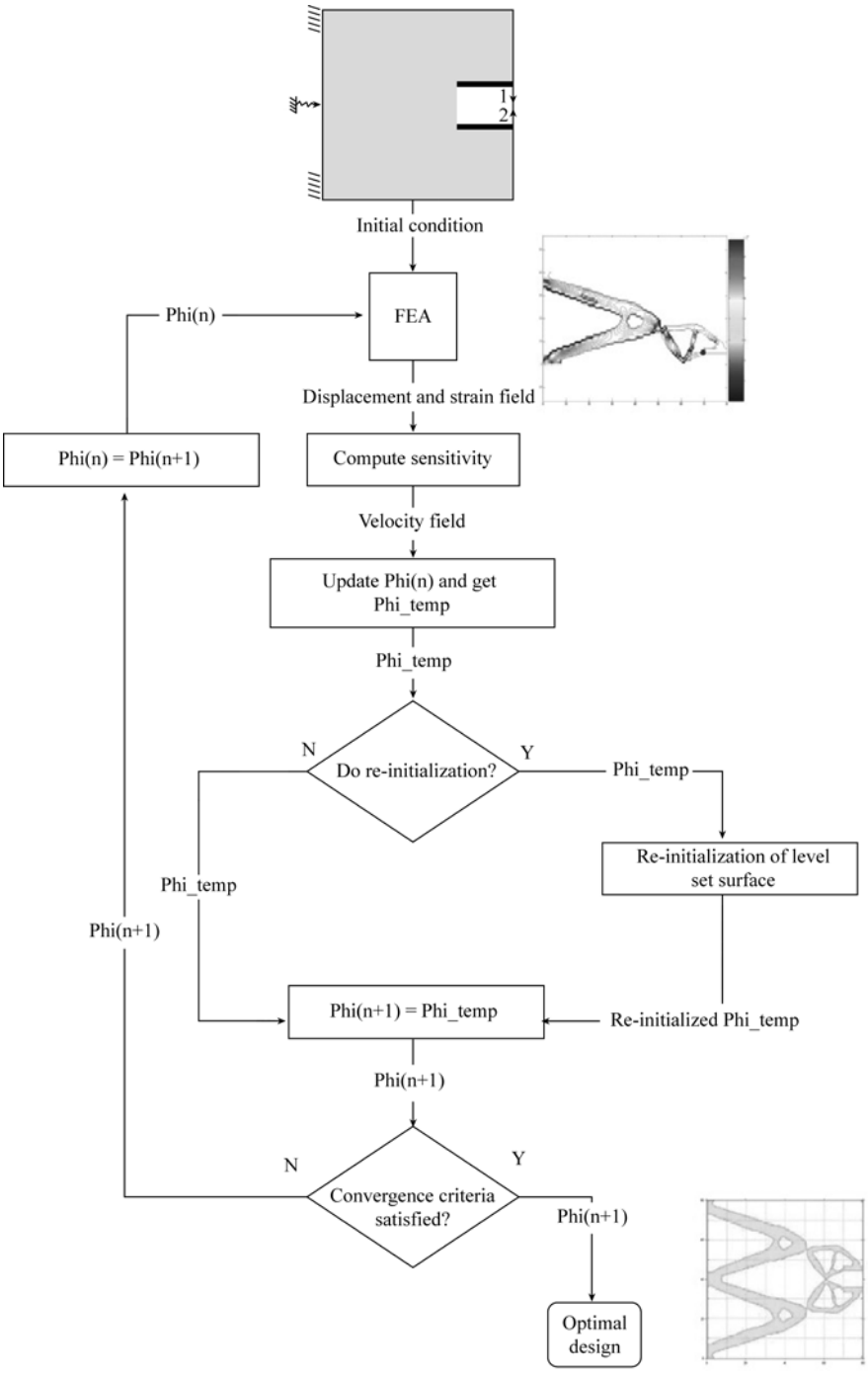

Fig. 19 A simple flowchart for the togology optimization

19.D. Peng, B. Merriman, S. Osher, H. Zhao and M. Kang A PDE-based local level set method, Journal of Computational Physics, 1999, 155, 410–438
20.G. Allaire, F. Jouve, A.-M. Toader, Structural optimization using sensitivity analysis and a level-set method, Journal of Computational Physics, 2004, 194(1): 363–393
21.G.K. Ananthasuresh, A new design paradigm for microelectro-mechanical systems and investigation on the compliant mechanism synthesis, Ph.D Thesis, University of Michigan, Ann Arbor, 1994
22.G.K. Lau, H. Du, M.K. Lim, Use of functional specifi-cations as objective functio
ns in topological optimizationof compliant mechanisms, Computer methods in applied mechanics and engineering, 2001, 190:4421–4433
23.M. Burger, Lecture Notes on Infinite-dimensional Optimization and Optimal Design, March, 2004
24.M. Y. Wang and X. M. Wang, PDE-driven level sets, shape sensitivity, and curvature flow for structural topology optimization, CMES: Computer Modeling in Engineering & Sciences, 2004, 6(4): 373–395

25.M. Y. Wang and X. M. Wang, 'Color' level sets: A multiphase level set method for structural topology optimization with multiple materials, Computer Methods in Applied Mechanics and Engineering, 2004, 193(6-8): 469–496
26.X. Wang, M. Y. Wang, and D. Guo, Structural shape and topology optimization in a level-set based framework of region representation, Structural and Multidisciplinary Optimization, 2004, 27(1-2): 1–19
27.M.Y. Wang, X. M. Wang, and D. M. Guo, A level set method for structural topology optimization, Computer Methods in Applied Mechanics and Engineering, 2003, 192(1-2):227–246
28.M. Burge, A framework for the construction of level set methods for shape optimization and reconstruction, Interfaces and Free Boundaries, 2003, 5: 301–329
29.S. Osher, R. Fedkiw, Level Sets Methods and Dynamic Implicit Surfaces, Springer, 2003
30.J. A. Sethian, Level Set Methods and Fast Marching Methods (2nd ed.), Cambridge University Press, 1999
31.J. Sokolowski, J. P. Zolesio, Introduction to Shape Optimization: Shape Sensitivity Analysis, Springer, 1992